52nd IEEE Conference on Decision and Control
December 10-13, 2013. Florence, Italy

The Estimation of Radial Temperature Distribution in Cylindrical Battery Cells under Unknown Cooling Conditions

Youngki Kim, Shankar Mohan, Jason B. Siegel, Anna G. Stefanopoulou and Yi Ding

Abstract— **The estimation of temperature inside a battery cell requires accurate information about the cooling condition even when the battery surface temperature is measured. This paper presents a model-based approach for estimating the temperature distribution inside a cylindrical battery under the unknown convective cooling condition. A reduced order thermal model using a polynomial approximation of the temperature profile inside the battery is used. A Dual Extended Kalman Filter (DEKF) is then applied for the identification of the convection coefficient and the estimation of the battery core temperature. Experimental results show that the proposed DEKF-based estimation method can provide an accurate prediction of the core temperature under the unknown cooling condition by measuring the battery current and voltage along with surface and ambient temperatures.**

I. INTRODUCTION

Lithium ion (Li-ion) batteries have been considered and used as one of the most favorable energy storage systems for the electrification of vehicles. Automotive applications require high current rates, high energy density and deep discharge capability. Li-ion batteries also have the advantages of minimal memory effect and broad operating ranges [1], [2]. However, the Li-ion battery performance, cycle life and capacity are adversely affected by sustained operation at sub zero temperature and at high temperature (over 45°C) [3]–[6]. This presents a recurring problem in automotive applications where batteries are exposed to large temperature variations with frequent high current discharge/charge rate that cause internal heating. Thus, being able to estimate and predict the temperature distribution within cells and across a pack is vital for formulating power management strategies that are mindful of the performance and thermal limitations of the battery.

Monitoring of the cooling system is critical to ensure safe and reliable battery operation. The performance of the cooling system can degrade due to various reasons such as dust on fan blades, partial blockage in pipes, motor/pump aging or a failure. When such degradations occur, the heat rejection decreases and can cause battery heating even at lower power demands. Therefore, it is important to identify the convective heat coefficient not only for estimating the temperature distribution inside the battery but also for adjusting the thermal management.

Y. Kim, J. Siegel, and A. Stefanopoulou are with the Department of Mechanical Engineering, University of Michigan, Ann Arbor, MI, 48109, USA {youngki,siegeljb,annastef}@umich.edu

S. Mohan is with the Department of Electrical Engineering, University of Michigan, Ann Arbor, MI, 48109 USA. elemsn@umich.edu

Y. Ding is with U.S. Army Tank Automotive Research, Development, and Engineering Center (TARDEC), Warren, Michigan, 48397 USA yi.ding8.civ@mail.mil

This paper considers a novel method for estimating the temperature distribution inside a cylindrical battery and the convective cooling condition at the same time. To achieve this goal, the computationally efficient thermal model for a cylindrical battery proposed in [7] is used. This modeling approach facilitates a systematic prediction of the core, the surface and the volume-averaged temperatures along with the volume-averaged temperature gradient. A Dual Extended Kalman Filter (DEKF) is then applied for the identification of the convection coefficient and the temperature distribution inside a cylindrical battery based on measured signals such as the battery current and voltage along with battery surface and ambient temperatures. The proposed method can be augmented with other existing battery thermal or power management strategies for the safe and robust operation.

This paper is organized as follows: Section II presents the convective heat transfer problem for a cylindrical battery and the reduced order thermal model. The sensitivity of temperature prediction to changes in model parameters is numerically analyzed in Section III. In Section IV, the adaptive estimator applying a DEKF for estimating the core temperature and identifying the convection coefficient is addressed. Section V presents and discusses experimental results, and conclusions are drawn in Section VI.

II. THERMAL MODEL FOR CYLINDRICAL BATTERIES

A cylindrical battery is fabricated by rolling a stack of thin-layered sheets comprised of a cathode material, a separator and an anode material. Figure 1(a) shows the schematic of a cylindrical battery under consideration, a 2.3 Ah 26650 Lithium-Iron-Phosphate ($LiFePO_4$). Due to this structure, it is reasonable to assume a radially uniform heat generation rate inside the battery with convective heat transfer at the surface [8]. Lumped parameters are used so that material properties such as the thermal conductivity, the density, and the specific heat coefficient are assumed to be constant in a homogeneous body. The thermal conductivity is one or two orders of magnitude higher in the axial direction than in the radial direction. Therefore, the temperature distribution in the axial direction will be more uniform [9], [10]. Under these assumptions, the heat transfer equation of the 1-D temperature distribution $T(r,t)$ and boundary conditions are

978-1-4673-5717-3/13/$31.00 ©2013 IEEE

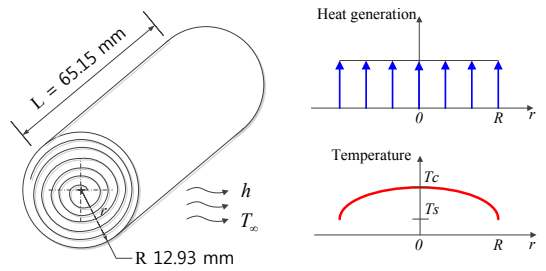

(a) (b)

Fig. 1. (a) Schematic for a A123 26650 cylindrical battery and (b) parabolic temperature profile under uniform heat generation

given by

$$\rho c_p \frac{\partial T(r,t)}{\partial t} = k_t \frac{\partial^2 T(r,t)}{\partial r^2} + \frac{k_t}{r}\frac{\partial T(r,t)}{\partial r} + \frac{Q(t)}{V_b}, \quad (1)$$

$$\text{B.C.'s } \frac{\partial T(r,t)}{\partial r}\Big|_{r=0} = 0, \quad (2)$$

$$\frac{\partial T(r,t)}{\partial r}\Big|_{r=R} = -\frac{h}{k_t}(T(R,t) - T_\infty), \quad (3)$$

where ρ, c_p and k_t represent the volume-averaged density, the specific heat coefficient, and the thermal conductivity of the battery respectively and are summarized in Table I. The radius of the battery is R, Q is the heat generation inside the battery, and V_b is the volume of battery. The ambient temperature and the convection coefficient are denoted by T_∞ and h, respectively. The boundary condition in Eq. (2) represents the symmetric structure of the battery about the core. The other boundary condition shown in Eq. (3) represents the convective heat transfer at the surface of the battery.

With evenly distributed heat generation rate, the temperature distribution along r-direction of the battery is assumed to satisfy the following polynomial approximation proposed in [11] (see Fig. 1(b))

$$T(r,t) = a(t) + b(t)\left(\frac{r}{R}\right)^2 + d(t)\left(\frac{r}{R}\right)^4,$$

where $a(t)$, $b(t)$, and $d(t)$ are time-varying constants.

The volume-averaged temperature $\bar{T}$ and temperature gradient $\bar{\gamma}$ are introduced as follows:

$$\bar{T} = \frac{2}{R^2}\int_0^R rT dr,$$
$$\bar{\gamma} = \frac{2}{R^2}\int_0^R r\left(\frac{\partial T}{\partial r}\right) dr.$$

The temperature distribution can be expressed as a function of $\bar{T}$, $\bar{\gamma}$ and the surface temperature T_s:

$$T(r,t) = 4T_s - 3\bar{T} - \frac{15R}{8}\bar{\gamma} + \left[-18T_s + 18\bar{T} + \frac{15R}{2}\bar{\gamma}\right]\left(\frac{r}{R}\right)^2 + \left[15T_s - 15\bar{T} - \frac{45R}{8}\bar{\gamma}\right]\left(\frac{r}{R}\right)^4. \quad (4)$$

The PDE (1) can be converted into ODEs by substituting Eq. (4) to following volume-averaged governing equation and its partial derivative with respect to r:

$$\int_0^R \left(\rho c_p \frac{\partial T(r,t)}{\partial t} - k_t \frac{\partial^2 T(r,t)}{\partial r^2} - \frac{k_t}{r}\frac{\partial T(r,t)}{\partial r} - \frac{Q(t)}{V_b}\right) dr = 0,$$
$$\int_0^R \frac{\partial}{\partial r}\left(\rho c_p \frac{\partial T(r,t)}{\partial t} - k_t \frac{\partial^2 T(r,t)}{\partial r^2} - \frac{k_t}{r}\frac{\partial T(r,t)}{\partial r} - \frac{Q(t)}{V_b}\right) dr = 0.$$

Finally, the two-state thermal model can be given by the following form:

$$\dot{x} = Ax + Bu,$$
$$y = Cx + Du, \quad (5)$$

where $x = [\bar{T}\ \bar{\gamma}]^T$, $u = [Q\ T_\infty]^T$ and $y = [T_c\ T_s]^T$ are states, inputs and outputs respectively. The variable T_c represents the temperature at the core of the battery ($r = 0$). System matrices A, B, C, and D are defined as follows:

$$A = \begin{bmatrix} \frac{-48\alpha h}{R(24k_t+Rh)} & \frac{-15\alpha h}{24k_t+Rh} \\ \frac{-320\alpha h}{R^2(24k_t+Rh)} & \frac{-120\alpha(4k_t+Rh)}{R^2(24k_t+Rh)} \end{bmatrix},$$
$$B = \begin{bmatrix} \frac{\alpha}{k_t V_b} & \frac{48\alpha h}{R(24k_t+Rh)} \\ 0 & \frac{320\alpha h}{R^2(24k_t+Rh)} \end{bmatrix},$$
$$C = \begin{bmatrix} \frac{24k_t-3Rh}{24k_t+Rh} & -\frac{120Rk_t+15R^2h}{8(24k_t+Rh)} \\ \frac{24k_t}{24k_t+Rh} & \frac{15Rk_t}{48k_t+2Rh} \end{bmatrix},$$
$$D = \begin{bmatrix} 0 & \frac{4Rh}{24k_t+Rh} \\ 0 & \frac{Rh}{24k_t+Rh} \end{bmatrix}. \quad (6)$$

The thermal diffusivity α is defined as follows:

$$\alpha = k_t/\rho c_p.$$

The heat generation rate Q can be calculated by the simplified form in [12] as following:

$$Q = i(U - V) - i\left(T\frac{\partial U}{\partial T}\right), \quad (7)$$

wherein the heat generation due to enthalpy-of-mixing, phase-change, and heat capacity are assumed to be negligible. The current, the open-circuit voltage, and the terminal voltage are i, U, and V, respectively.

In this paper, the heat generation due to entropy change,

TABLE I
PARAMETERS OF THE BATTERY [7]

Parameter	Symbol	Value	Unit
Density	ρ	2047	kg/m^3
Specific heat coeff.	c_p	1109	J/kg-K
Thermal conductivity	k_t	0.610	W/m-K
Radius	R	12.93e-3	m
Height	L	65.15e-3	m
Volume	V_b	3.4219e-5	m^3

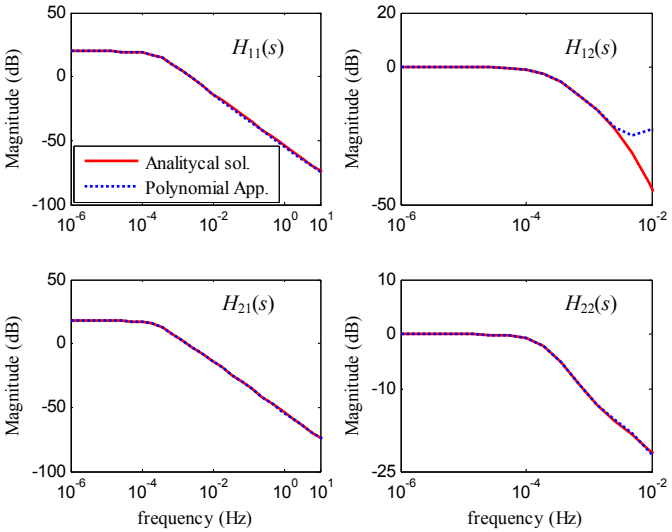

Fig. 2. Comparison of frequency response functions between analytical solution and polynomial approximation

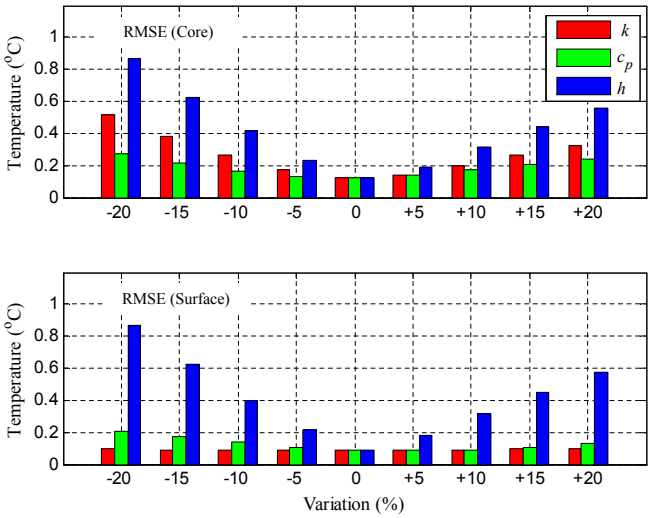

Fig. 3. The effect of parameter variation to the prediction of core and surface temperatures

the last term in (7), is neglected for simplicity. This simplification is warranted since the typical operating range for state-of-charge in a hybrid electric vehicle (HEV) is narrow, and $\frac{\partial U}{\partial T}$ is insignificant as shown in [13] for this chemistry. In addition, the reversible entropic heat generation would have zero mean value when the battery is operating in charge-sustaining mode, typical of HEV operation.

The frequency response of the transfer function for the reduced order model, $H(s) = D + C(sI - A)^{-1}B$, is compared to that of the analytical solution in [14]. The identity matrix and Laplace variable are presented by I and s, respectively. Parameters used to generate the plots in Fig. 2 are summarized in Table I. The heat transfer coefficient of h=25W/m^{2}K is chosen since this value is typical of forced-air convection condition [15].

Figure 2 shows that the effects of heat generation rate on the core and the surface temperatures, denoted by $H_{11}(s)$ and $H_{21}(s)$ respectively, can be accurately predicted over the whole range of frequency. On the other hand, the responses of the core and the surface temperatures excited by the ambient temperature, $H_{12}(s)$ and $H_{22}(s)$ respectively, are nearly identical to the analytical solution for frequencies below 10^{-2} Hz. In general, the temperature of the cooling media does not change rapidly; thus, the prediction of temperature distribution using the proposed approach can be considered reasonably accurate.

III. PARAMETER SENSITIVITY ANALYSIS

Three parameters, the thermal conductivity k_t, the specific heat coefficient c_p and the convection coefficient h, are chosen for the sensitivity analysis. To investigate the impact of variations in parameters on the performance of temperature prediction, each parameter is varied between -20% to 20% around the nominal value while holding the other parameters constant. Figure 3 shows that the thermal conductivity and the specific heat coefficient have more influence on the prediction of the core temperature than the surface temperature. This result corresponds to the fact that the heat generated inside the battery is transferred through conduction. On the other hand, the prediction of the surface temperature is the most sensitive to the variation of the convection coefficient, which can be explained by the fact that the convection coefficient is directly related to the convective boundary condition Eq. (3). The convection coefficient has the most significant influence on the overall prediction of the core and the surface temperatures.

The specific heat coefficient and the thermal conductivity are weakly dependent on temperature [13], [16], [17], so the assumption of constant parameters can be justified. On the other hand, the convection coefficient is highly dependent on fan speed or fluid velocity as expressed by empirical correlations provided by Zukauskas [18]. Consequently, the accurate identification of the convection coefficient is important for better prediction of temperature inside the battery. This importance justifies the on-line identification of the convection coefficient for better estimation of temperature as detailed in Section IV.

IV. ESTIMATION OF TEMPERATURE AND CONVECTION COEFFICIENT

As discussed in section III, the estimation of temperature inside the battery requires accurate knowledge of the convection coefficient which depends on the cooling condition. In order to identify the convection coefficient and the core temperature inside the battery on-line, a Dual Extended Kalman filter (DEKF) in [19] is applied. The other thermal parameters such as the thermal conductivity and the specific heat coefficient are constant since these parameters have less influence on temperature and do not change significantly over time.

Assuming the input $u(t)$ is constant over each sampling interval ΔT, a parameter varying (PV) discrete-time model

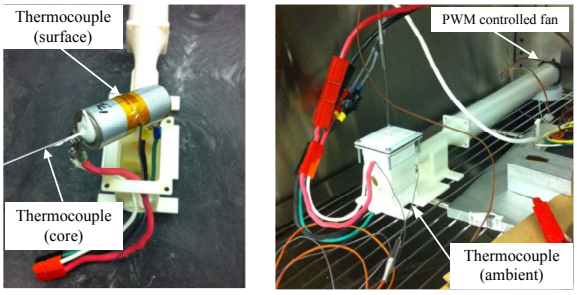

Fig. 4. Experimental setup for temperature measurement

at time step k can be obtained as

$$\begin{aligned} x_{k+1} &= \bar{A}(\theta_k)x_k + \bar{B}(\theta_k)u_k + w_k, \\ y_k &= C(\theta_k)x_k + D(\theta_k)u_k + v_k, \\ \theta_{k+1} &= \theta_k + r_k, \end{aligned} \tag{8}$$

where $x = [\bar{T}\ \bar{\gamma}]^T$, $y = T_s$, $\theta = h$, and $u = [Q\ T_\infty]^T$. System matrices $\bar{A} \approx I + A\Delta T$ and $\bar{B} = B\Delta T$ are obtained from matrices in Eq. (6). Noise signals w_k, v_k and r_k, are independent, zero-mean, Gaussian processes of covariance matrices Σ_w, Σ_v, and Σ_r, respectively.

The design of the DEKF estimator is given as following update processes.

Time update for the parameter filter:

$$\begin{aligned} \hat{\theta}_k^- &= \hat{\theta}_{k-1}^+, \\ S_k^- &= S_{k-1}^+ + \Sigma_r. \end{aligned}$$

Time update for the state filter:

$$\begin{aligned} \hat{x}_k^- &= \bar{A}_{k-1}\hat{x}_{k-1}^+ + \bar{B}_{k-1}u_{k-1} \\ P_k^- &= \bar{A}_{k-1}P_{k-1}^+\bar{A}_{k-1}^T + \Sigma_w. \end{aligned}$$

Measurement update for the state filter:

$$\begin{aligned} K_k &= P_k^- C_k^{xT}\left[C_k^x P_k^- C_k^{xT} + \Sigma_v\right]^{-1}, \\ \hat{x}_k^+ &= \hat{x}_k^- + K_k\left[y_k - C(\hat{\theta}_k^-)\hat{x}_k^- - D(\hat{\theta}_k^-)u_k\right] \\ P_k^+ &= \left[I - K_k C_k^x\right]P_k^-. \end{aligned}$$

Measurement update for the parameter filter:

$$\begin{aligned} L_k &= S_k^- C_k^{\theta T}\left[C_k^\theta P_k^- C_k^{\theta T} + \Sigma_e\right]^{-1}, \\ \hat{\theta}_k^+ &= \hat{\theta}_k^- + L_k\left[y_k - C(\hat{\theta}_k^-)\hat{x}_k^- - D(\hat{\theta}_k^-)u_k\right] \\ S_k^+ &= \left[I - L_k C_k^\theta\right]S_k^-, \end{aligned}$$

where superscripts $-$ and $+$ denote the *a priori* and *a posteriori* values respectively. The matrices $\bar{A}_{k-1}$, C_k^x and C_k^θ are calculated according to

$$\begin{aligned} \bar{A}_{k-1} &= \bar{A}(\theta_k)|_{\theta_k=\hat{\theta}_k^-}, \\ C_k^x &= C(\theta_k)\Big|_{\theta_k=\hat{\theta}_k^-}, \\ C_k^\theta &= \frac{dy_k}{d\theta_k}\Big|_{x_k=\hat{x}_k^-,\theta_k=\hat{\theta}_k^-}. \end{aligned}$$

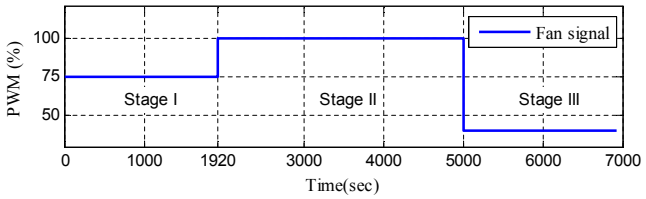

Fig. 5. Fan schedule for forced-air convective cooling

The identified states $\hat{x}$ and parameter $\hat{\theta}$, computed from the above DEKF algorithm, are used to estimate the core temperature in the battery from Eq. (5). It is noted that since the thermal system is linear, the DEKF becomes a Kalman Filter (KF) when the parameter of the convection coefficient is known or given.

V. EXPERIMENTAL RESULTS

In this section, the performance of the proposed temperature estimator using the DEKF is compared with that of the baseline KF estimator without parameter identification. Following the experimental set-up in [20] as shown in Fig. 4, we draw a current and measure voltage and temperatures at the core and the surface of the battery while controlling the ambient temperature in the thermal chamber. Thermocouples used for temperature measurements are T-type whose accuracy is the maximum of 0.5°C or 0.4% only according to technical information from the manufacturer, OMEGA. The surface temperature is used for the estimator and the core temperature is measured to verify the estimation accuracy. The experiment is performed using the Escort Convoy Cycle (ECC) [7] while controlling the cooling condition. Three different forced convective cooling conditions (stage I, stage II, and stage III) are achieved by using different Pulse Width Modulation (PWM) signals driving the fan as shown in Fig. 5 which corresponds to an increase, followed by a decrease in the coolant flow rate. In order to investigate the influence of change in the parameter on the temperature estimation, the parameter is provided to each estimator as following:

- In stage I, the off-line predetermined convection coefficient is provided to the KF and is used for the DEKF as an initial value: $\tilde{\theta} = \theta^*$ and $\hat{\theta}(0) = \theta^*$
- In stage II, the off-line predetermined convection coefficient is provided to the KF only: $\tilde{\theta} = \theta^*$
- In stage III, two times larger convection coefficient compared to the known value is provided to the KF: $\tilde{\theta} = 2\theta^*$

where $\tilde{\theta}$ and $\hat{\theta}$ denote fixed and identified parameters for the KF and the DEKF respectively whereas θ^* presents the predetermined parameter value. Other thermal properties such as the thermal conductivity and the specific heat coefficient are assumed constant with values provided in Table I.

It is assumed that the initial temperature distribution inside the battery is uniform at 30°C and the convection coefficient is 56.2 W/m^{2}K, i.e. $\hat{x}(0) = [30\ 0]^T$ and $\hat{\theta}(0) = 56.2$ respectively. The covariance matrix for the state $\Sigma_w = {\beta_1}^2\text{diag}(1,1)$ describes the process noise where $\beta > 0$ is a parameter for tuning based on the model inaccuracy.

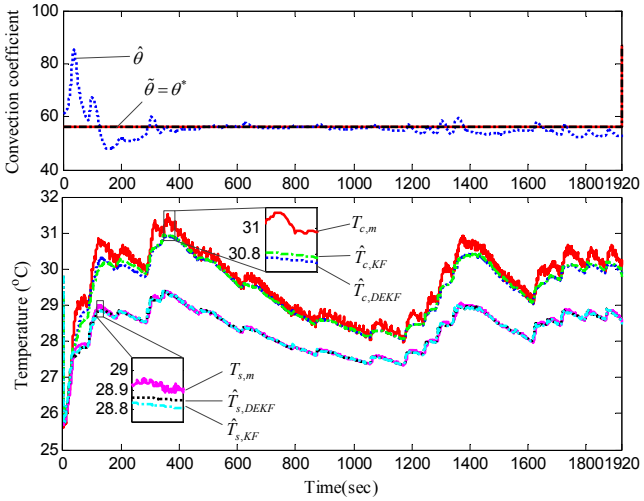

Fig. 6. Comparison of performance between KF estimator, DEKF estimator during stage I: convection coefficient (top) and temperature (bottom)

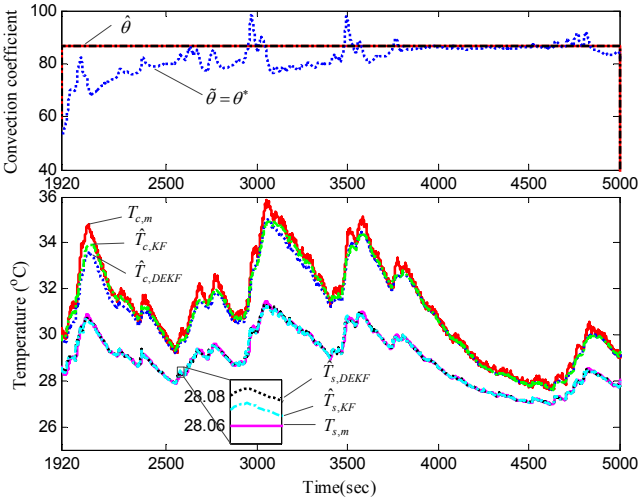

Fig. 7. Comparison of performance between KF estimator, DEKF estimator during stage II: convection coefficient (top) and temperature (bottom)

The noise covariance $\Sigma_v = \sigma^2$ is determined from the standard deviation of temperature signal, $\sigma = 0.05°\text{C}$. The covariance matrix for the parameter $\Sigma_r = {\beta_2}^2$ influences the performance of noise filtering and the rate of parameter convergence. Ultimately, the initial conditions of the error covariance matrices and tuning parameters are chosen as $P(0) = \text{diag}(1, 1)$, $\beta_1 = 0.0005$, $S(0) = 1$, and $\beta_2 = 0.01$ through repeated simulations.

The results for the parameter and state estimation are shown in Fig. 6–8 and are summarized in Table II. Figure 6 shows that the closed-loop estimators can accurately predict temperature inside the battery. Even though the identified value is used as an initial guess for the parameter, a large deviation of the identified parameter is observed in the initial time periods. This deviation is caused by the error in the initial states. Nevertheless, the on-line identified parameter is close to the off-line determined value. Therefore, the performance of the DEKF estimator is comparable to that of the KF estimator. In particular, the RMSE for the core temperature estimation by the DEKF is 0.26, the same RMSE by the KF. Despite a slight error between the measured and estimated temperatures, the closed-loop estimators show a good performance in predicting the core temperature overall.

Figure 7 illustrates the performance of temperature estimation by the closed-loop estimator in stage II when there is a sudden change in the cooling condition. The KF can accurately estimate the core temperature with information about the change in parameter value. Since the DEKF is capable of compensating inaccuracy in the parameter of the system, the DEKF provides reasonably an accurate estimate for the core temperature compared to the core temperature predicted by the KF. The RMSE for the core temperature estimation by DEKF is slightly larger than the RMSE by the KF, which is caused by the errors during initial time periods before the parameter converges to the true value. Nevertheless, the error is still reasonably small considering the sensor accuracy.

As seen from Fig. 8, the KF overestimates the core temperature when the incorrect parameter value is used as the convection coefficient. In other words, the reliable estimation of the core temperature is only possible when accurate parameter values are available. Thus, it can be concluded

TABLE II

PERFORMANCE OF TEMPERATURE ESTIMATION: RMSES FOR CORE AND SURFACE

Method	DEKF		KF	
Location	Core	Surface	Core	Surface
Stage I	0.26	0.07	0.26	0.07
Stage II	0.39	0.08	0.29	0.08
Stage III	0.31	0.11	1.18	0.15

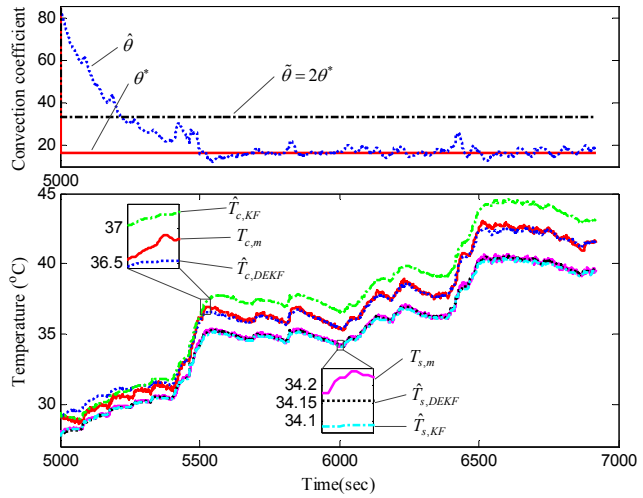

Fig. 8. Comparison of performance between KF estimator, DEKF estimator during stage III: convection coefficient (top) and temperature (bottom)

that the DEKF outperforms the KF due to the capability of parameter identification. The RMSE for the core temperature estimation in stage III can be substantially reduced from 1.18 to 0.31 by the DEKF.

It is worth noting that the DEKF can be augmented with other existing fault detection methods and power management strategies to improve the system robustness without cost increase. For instance, in order to detect partial blockage in cooling system, typically, a mass flow or pressure sensor is required. The DEKF enables the identification of the convection coefficient by using sensors which are already instrumented at the battery. The identified parameter can be also used for monitoring the malfunction or degradation of cooling system. Under the assumption that the relationship between the convection coefficient and fan speed or PWM signal is known, the malfunction of the cooling system can be detected by comparing the identified parameter with the known value. When the difference between the identified and predetermined values $|\hat{\theta}-\theta^*|$ is bounded and small, it can be considered that there is no fault in the cooling system. On the other hand, $|\hat{\theta}-\theta^*| \gg \epsilon$ where ϵ is a pretuned threshold, a cooling fault can be detected. Furthermore, $|(\hat{\theta}-\theta^*)/\theta^*|$ can be interpreted as the severity of degradation of the cooling system.

VI. CONCLUSION

In this study, a method to estimate the temperature distribution in a cylindrical battery under the unknown cooling condition is proposed. First, a reduced order thermal model using a polynomial approximation is used to predict a radial temperature profile. The numerical analysis on parameter sensitivity supports the use of constant parameters for the thermal conductivity and the specific heat coefficient and the importance of identifying the convection coefficient online. Then, a Dual Extended Kalman Filter is applied to estimate the core temperature of the battery and the convection coefficient by the cooling fan. The proposed method requires no knowledge of the convective cooling condition. The results show that the proposed DEKF can provide reasonably accurate estimates of the core temperature and the convection coefficient by using the current, the voltage, the battery surface and ambient temperatures. In addition, faulty operation of the cooling system can be detected by monitoring the difference between the identified and off-line predetermined values. Since forced air is used as a cooling media to reject heat from the battery in this paper, the range of the convection coefficient of which we are interested is less than 100 W/m^{2}K. Therefore, the reader is urged to investigate whether the polynomial approximation is valid for their applications.

In the future, the proposed method can be used to develop various battery management strategies, e.g. the determination of maximum current with consideration of thermal constraints or optimal fan scheduling for energy efficiency, leading to the safe and efficient operation of the battery system.

VII. ACKNOWLEDGMENTS

The authors wish to acknowledge the technical and financial support of the Automotive Research Center (ARC) in accordance with Cooperative Agreement W56HZV-04-2-0001 U.S. Army Tank Automotive Research, Development and Engineering Center (TARDEC) Warren, MI. UNCLASSIFIED: Distribution A. Approved for public release.

REFERENCES

[1] R. Huggins, *Advanced Batteries: Materials Science Aspects, first edition*. Springer, 2008.

[2] Z. Rao and S. Wang, "A review of power battery thermal energy management," *Renewable and Sustainable Energy Reviews*, vol. 15, no. 9, pp. 4554–4571, 2011.

[3] J. Shim, R. Kostecki, T. Richardson, X. Song, and K. Striebel, "Electrochemical analysis for cycle performance and capacity fading of a lithium-ion battery cycled at elevated temperature," *Journal of Power Sources*, vol. 112, no. 1, pp. 222 – 230, 2002.

[4] X. Zhang, P. Ross, R. Kostecki, F. Kong, S. Sloop, J. Kerr, K. Striebel, E. Cairns, and F. McLarnon, "Diagnostic characterization of high power lithium-ion batteries for use in hybrid electric vehicles," *Journal of the Electrochemical Society*, vol. 148, no. 5, pp. 463–70, 2001.

[5] G. M. Ehrlich, "Lithium-ion batteries," in *Handbook of Batteries, third edition*, ch. 35, McGraw-Hill, 2002.

[6] S. Zhang, K. Xu, and T. Jow, "Low temperature performance of graphite electrode in li-ion cells," *Electrochimica Acta*, vol. 48, no. 3, pp. 241 – 246, 2002.

[7] Y. Kim, J. B. Siegel, and A. G. Stefanopoulou, "A computationally efficient thermal model of cylindrical battery cells for the estimation of radially distributed temperatures," in *American Control Conference*, (Washington, DC, USA), June 17-19 2013.

[8] D. R. Pendergast, E. P. DeMauro, M. Fletcher, E. Stimson, and J. C. Mollendorf, "A rechargeable lithium-ion battery module for underwater use," *Journal of Power Sources*, vol. 196, no. 2, pp. 793–800, 2011.

[9] H. Maleki, S. A. Hallaj, J. R. Selman, R. B. Dinwiddie, and H. Wang, "Thermal properties of lithium-ion battery and components," *Journal of The Electrochemical Society*, vol. 146, no. 3, pp. 947–954, 1999.

[10] S. Chen, C. Wan, and Y. Wang, "Thermal analysis of lithium-ion batteries," *Journal of Power Sources*, vol. 140, no. 1, pp. 111–124, 2005.

[11] V. R. Subramanian, V. D. Diwakar, and D. Tapriyal, "Efficient macro-micro scale coupled modeling of batteries," *Journal of the Electrochemical Society*, vol. 152, no. 10, pp. A2002 – A2008, 2005.

[12] D. Bernardi, E. Pawlikowski, and J. Newman, "General energy balance for battery systems," *Journal of the Electrochemical Society*, vol. 132, no. 1, pp. 5–12, 1985.

[13] C. Forgez, D. Vinh Do, G. Friedrich, M. Morcrette, and C. Delacourt, "Thermal modeling of a cylindrical $LiFePO_4$/graphite lithium-ion battery," *Journal of Power Sources*, vol. 195, no. 9, pp. 2961 – 2968, 2010.

[14] M. Muratori, N. Ma, M. Canova, and Y. Guezennec, "A model order reduction method for the temperature estimation in a cylindrical li-ion battery cell," in *Proceedings of the ASME Dynamic Systems and Control Conference*, vol. 1, pp. 633–640, 2010.

[15] J. Shi, F. Wu, S. Chen, and C. Zhang, "Thermal analysis of rapid charging nickel/metal hydride batteries," *Journal of Power Sources*, vol. 157, no. 1, pp. 592–599, 2006.

[16] H. Maleki, J. Selman, R. Dinwiddie, and H. Wang, "High thermal conductivity negative electrode material for lithium-ion batteries," *Journal of Power Sources*, vol. 94, no. 1, pp. 26–35, 2001.

[17] K. Onda, T. Ohshima, M. Nakayama, K. Fukuda, and T. Araki, "Thermal behavior of small lithium-ion battery during rapid charge and discharge cycles," *Journal of Power Sources*, vol. 158, no. 1, pp. 535–542, 2006.

[18] A. Zukauskas, "Heat transfer from tubes in crossflow," vol. 8 of *Advances in Heat Transfer*, pp. 93–160, Academic Press, 1972.

[19] E. A. Wan and A. T. Nelson, *Dual Extended Kalman Filter Methods*, pp. 123–173. John Wiley & Sons, Inc., 2002.

[20] X. Lin, H. Perez, J. Siegel, A. Stefanopoulou, Y. Li, R. Anderson, Y. Ding, and M. Castanier, "Online parameterization of lumped thermal dynamics in cylindrical lithium ion batteries for core temperature estimation and health monitoring," *Control Systems Technology, IEEE Transactions on*, vol. 21, no. 5, pp. 1745–1755, 2013.